A State-Space Framework for Movement Control to Dynamic Goals Through Brain-Driven Interfaces

Lakshminarayan Srinivasan*, *Member, IEEE*, and Emery N. Brown, *Senior Member, IEEE*

***Abstract*—State-space estimation is a convenient framework for the design of brain-driven interfaces, where neural activity is used to control assistive devices for individuals with severe motor deficits. Recently, state-space approaches were developed to combine goal planning and trajectory-guiding neural activity in the control of reaching movements of an assistive device to static goals. In this paper, we extend these algorithms to allow for goals that may change over the course of the reach. Performance between static and dynamic goal state equations and a standard free movement state equation is compared in simulation. Simulated trials are also used to explore the possibility of incorporating activity from parietal areas that have previously been associated with dynamic goal position. Performance is quantified using mean-square error (MSE) of trajectory estimates. We also demonstrate the use of goal estimate MSE in evaluating algorithms for the control of goal-directed movements. Finally, we propose a framework to combine sensor data and control algorithms along with neural activity and state equations, to coordinate goal-directed movements through brain-driven interfaces.**

***Index Terms*—Goal-directed movement, neural prosthetic device, recursive estimation, state equation.**

I. Introduction

SEVERAL neurological conditions dramatically restrict voluntary movement, including amyotrophic lateral sclerosis, spinal cord injury, brainstem infarcts, advanced-stage muscular dystrophies, and diseases of the neuromuscular junction. A growing set of technologies is being developed to allow brain-driven control of assistive devices for individuals with severe motor deficits. Variously called brain-machine interfaces [1], [2], motor neural prostheses [3]–[5], and cognitive prostheses [6], [7], they represent a communication link that bypasses affected channels of motor output.

Many alternative technologies are available that utilize remaining motor function rather than neural activity to generate control signals. Movements of the eye or tongue can be tracked to control a cursor. Suction on a straw can navigate a wheelchair. Contractions or electromyographic signals of larger muscle groups such as the platysma or pectoralis major can be monitored to activate joints in a prosthetic arm [8]. Volitional grasping with a prosthetic hand can be achieved through mechanical cabling to the contralateral shoulder [9]. Although they represent practical solutions for many patients, these alternatives provide restricted control to any user. Moreover, they may not be feasible for individuals with profound motor deficits.

Brain-driven interfaces have the potential to provide users with control that is more dexterous, natural to use, and less susceptible to fatigue than existing muscle-based alternatives. In principle, these interfaces would be available even for individuals with near-complete loss of voluntary motor function, such as with locked-in syndrome where only blinking and vertical gaze remain.

The four common elements of existing brain-driven interfaces are a method to monitor neural activity, an algorithm to map this activity to control signals, a device to be controlled, and a feedback mechanism that informs the user about the state of the device. Monitoring approaches provide spatial resolution and broader frequency bands at the expense of more invasive electrode placement. Scalp leads provide waveforms up to 40 Hz, integrating activity from square-centimeters of cortex [10]. Subdural leads provide electrocorticographic (ECoG) signals up to 200 Hz that are collected from an estimated area of fractions of a square millimeter [10]. Cortical electrode arrays have access to local field potentials similar to EcoG, but also monitor action potentials, which are transient 1 ms electrical spikes from micrometer-scale neurons. These arrays typically record from tens but up to hundreds of individual neurons spread over one square millimeter. Signal preprocessing is typically employed in all of these approaches, including bandpass filtering and spike sorting [11]–[14], where action potentials are grouped by shape in an effort to localize spiking events to distinct neurons. Various algorithms can then be employed to map neural signals to control signals. This mapping can be made adaptive, changing so as to minimize performance errors even as neurons fade out [15] and the subject learns to use the interface. Feedback in existing prototypes is predominantly limited to visualization of the device state and juice rewards [3]–[7], or auditory cues, but somatosensory cortical electrodes have also been proposed.

Challenges remain on all fronts in the design of brain-driven interfaces. Cortical electrode arrays have only preliminarily been evaluated for chronic recording in humans [16]. To endure long-term use, monitoring approaches must achieve low power consumption, mechanical stability, biocompatibility, and otherwise reliable access to relevant neural signals. Movements

Manuscript received March 5, 2006; revised August 26, 2006. The work of L. Srinivasan was supported in part by the National Institutes of Health (NIH) under Medical Scientist Training Program Fellowship T32 GM07753-27. The work of E. N. Brown was supported in part by the NIH under Grant R01 DA015644 to ENB. *Asterisk indicates corresponding author.*

*L. Srinivasan was with the Laboratory for Information and Decision Systems, Department of Electrical Engineering and Computer Science, Massachusetts Institute of Technology (MIT), Cambridge, MA 02139 USA. He is now with the Center for Nervous System Repair, Department of Neurosurgery, Massachusetts General Hospital, 50 Blossom Street, EDR-410, Boston, MA 02114 USA and the Harvard/MIT Division of Health Sciences and Technology, 77 Massachusetts Ave., E25–519, Cambridge, MA 02139 USA (e-mail: ls2@mit.edu).

E. N. Brown is with the Neuroscience Statistics Research Laboratory, Department of Anesthesia and Critical Care, Massachusetts General Hospital, Charlestown, MA 02129 USA, and also with the Division of Health Sciences and Technology and the Department of Brain and Cognitive Sciences, MIT, Cambridge, MA 02139 USA.

Digital Object Identifier 10.1109/TBME.2006.890508

generated by existing prototypes are either slow and deliberate, or fast and uncontrolled. The evaluation of learning is not standardized. Reported training times range from minutes [2] to months [1] for acquiring proficiency with a device, depending on the device and method of performance evaluation. Algorithms must be developed to enable increased dexterity, faster learning, and robust performance. Finally, the optimization of real time feedback and training regimens is largely unexplored.

The mapping of preprocessed neural activity to control signals is typically approached as an estimation problem, where the algorithm seeks to track the user's hidden intention based on neural activity that serves as a noisy observation of that intention. The development of these mappings parallels the earlier development of estimation procedures in electrical engineering and later applications to neurophysiology: manually adjusted linear combinations of power spectral band energies [17], population vectors for automated but sub-optimal linear mappings [18], linear regression for optimized linear mappings [19], and most recently, recursive Bayesian estimation procedures [20]–[22]. This last advance in particular has allowed dramatically better tracking than linear regression in off-line data analyses [23]. In decoding trajectories or sequences of intentions, this improvement is largely due to the introduction of a state equation, a mathematical expression of underlying structure in the intention, such as continuity. Variants have evolved to progressively account for the true statistical nature of spiking activity: the Kalman filter [22], particle filter [20], and point process filter [21]. Bayesian estimation [6], [7], support vector machines, and other classification methods have also been used with neural observations of discrete intentions such as icon selection from an on-screen menu.

Reaching movements are one class of intentions that a user may seek to specify. An intended reaching motion is comprised of a trajectory of states from some initial state to a final state, or goal. Estimation procedures typically employ neural activity as a concurrent observation of the intended state in the path, such as velocity-related primary motor cortical activity. Neural activity has also separately been characterized in goal planning brain regions such as posterior parietal cortex (PPC) or premotor cortex to estimate discrete goals for icon selection. However, these observations had not been incorporated into the recursive estimation of the reach trajectory until recently, when state equations were developed to incorporate both path and goal related neural activity [24]–[27].

In simulation, the trajectory reconstructions resulting from these static-goal state equations that combined path and goal activity were more accurate than either path or goal related activity could provide alone. One approach began with a state equation for free arm movement, called a free movement state equation, and probabilistically conditioned the state equation on the final state [26], [28]. Another approach employed a state equation that corresponded to the solution to the LQ control problem [25]. For the appropriate parameter choices, both approaches defined state equations with identical average trajectories. However, the variance in the increments differed between the methods, shaping the way in which the user controlled deviations from the average trajectory.

In both approaches [25], [28], the goal of the trajectory was modeled to be static. However, humans need to be capable of changing goals over the course of a reach, such as when adjusting for an unexpected bounce of a baseball. The delay in making corrective movements approaches that of visual reaction times, suggesting that goals can be changed rapidly based on visual cues even while the reach is being executed [29], [30]. Static goals also necessitate path corrections [31], where remembered target location is employed early in the movement and visual information is incorporated later in the movement to refine estimates of the goal.

Interception of a moving target along a straight path does not necessitate a changing goal. In one experiment [32], fast target movements resulted in unimodal hand velocity profiles, suggesting one directed motion to a static goal, the expected location of the target. However, goals may change even with targets that move along straight paths. In the same experiment, slower movements elicited a multimodal hand velocity, suggesting a sequence of submovements that relate to a dynamic goal, possibly an updated estimate of the expected target location.

Recent evidence suggests that the PPC is involved in representing a dynamic goal. Transcranial magnetic stimulation over the left PPC during a reach to a moving target results in persistence towards the original target location [33]. Primate electrophysiology demonstrates that PPC target tuning shifts with gaze direction [6], [34]. Spiking activity in parietal area 7a correlates with aspects of a moving target on trials when a monkey is instructed to withhold from reaching [29]. Functional magnetic resonance imaging suggests that this gaze-centered activity is updated with eye movements during reach planning [35]. Patients with lesions to the PPC are unable to dynamically update goal representations to adjust for eye movements, resulting in optic ataxia [36].

Monitoring technologies that are located in proximity to such goal planning regions will have access to dynamic goal information. In this paper, we present a method to incorporate this additional information and to allow for goals that change over the duration of the reach, expanding on concepts introduced in [26], [28], and [37]. First, we develop a dynamic goal state equation by building on the static case [26], [28] with a graphical model. Next, sample trajectories are generated to visualize the structure imposed by this state equation. Finally, performance is compared between point process estimation procedures that use the static goal, dynamic goal, and free movement state equations under a range of goal dynamics.

II. Theory

In this section, we derive the dynamic goal state equation from the static case that was addressed previously [26], [28]. A state equation specifies a prior distribution on the sequence of arm states $(x_0, x_1, \ldots, x_T)$ that form a trajectory. The simplest free arm movement state equation is linear with Gaussian additive noise, where x_t is a $n \times 1$ vector describing the arm state at time step t, A_t is a $n \times n$ matrix, and w_t is a $n \times 1$ Gaussian random vector, referred to as an increment

$$x_{t+1} = A_t x_t + w_t. \tag{1}$$

In a probabilistic interpretation, this state equation is equivalent to the state transition density, denoted

$$p(x_{t+1}|x_t). \tag{2}$$

In reaching movements, we may also desire estimates of the static goal state z, defined as

$$z = x_T. \tag{3}$$

Prescient observations of the static goal state z have been demonstrated in PPC and premotor cortex. To incorporate neural observations of the static goal state, we previously [28] derived the new state transition density

$$p(x_{t+1}, z | x_t, z). \tag{4}$$

The corresponding state equation represents the evolution of a state vector that is augmented to include the goal state

$$\begin{pmatrix} x_{t+1} \\ z \end{pmatrix} = \begin{pmatrix} \Psi & \Gamma \\ 0 & I \end{pmatrix} \begin{pmatrix} x_t \\ z \end{pmatrix} + \begin{pmatrix} \varepsilon_t \\ 0 \end{pmatrix} \tag{5}$$

where

$$\Psi = [I - Q_t \Pi^{-1}(t,T)] A_t \tag{6}$$

$$\Gamma = Q_t \Pi^{-1}(t,T) \phi(t,T) \tag{7}$$

and

$$\phi(t,s) = \begin{cases} \prod_{i=1+\min(t,s)}^{\max(t,s)} A_i^{\operatorname{sign}(t-s)}, & t \neq s \\ I, & t = s \end{cases} \tag{8}$$

$$Q_t = \operatorname{cov}(w_t | x_t) \tag{9}$$

$$\Pi(t-1,T) = \phi(t-1,t)\Pi(t,T)\phi'(t-1,t) + \phi(t-1,t) Q_{t-1} \phi'(t-1,t) \tag{10}$$

$$\Pi(T,T) = Q_T. \tag{11}$$

This is the static goal state equation was derived in [28]. The random variable z that denotes the desired goal does not vary with time.

How can this state equation be used to generate reaching movements? The state equation represents our prior knowledge about the set of movements the user might want to generate, and the frequency with which those movements are generated. For example, the static goal state equation generates trajectories that look like reaching movements when the movement goal is known to the algorithm, but reduces to free movement trajectories when the goal location is highly uncertain. Recursive Bayesian filtering algorithms like the Kalman filter [22], particle filter [20], and point process filter [21] combine the state equation with neural signals such as local field potentials or ensemble spiking activity from groups of neurons to generate realtime estimates of the intended arm movement. See the Appendix for a summary of filters that work with ensemble spiking activity or field potentials.

We now develop a state equation that supports a dynamically evolving goal, beginning with the same free movement state equation given in (1). As general linear state equations had been assigned for free arm movements, we consider an analogous state equation on goal evolution to support a general class of goal movements

$$z_{t+1} = B_t z_t + \eta_t. \tag{12}$$

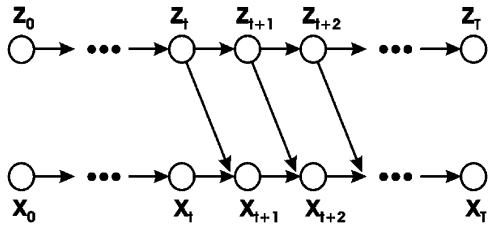

Fig. 1. Graphical model depicting the dynamic goal state equation. Nodes in this graph represent the desired goal z_t and trajectory state x_t at time step t. Edges specify the statistical dependence between state variables. When conditioned on all parents, a given node is independent of any other node. This graph structure indicates that the goal evolves independently of the path, the initial goal and path states are independent random variables, and the state x_{t+1} depends on the desired goal z_t and path state x_t of the previous time step.

We must now constrain the evolving path x_t to move to the evolving goal z_t in a way that generates a consistent prior distribution on the full set of random variables $(x_0, x_1, \ldots, x_T, z_0, z_1, \ldots, z_T)$. The interdependence between x_t and z_t is not otherwise arbitrary: we assume that the path at any given time evolves as if moving toward the current goal.

Graphical models on directed acyclic graphs provide a simple and systematic prescription for generating this consistent prior distribution. Consider the diagram in Fig. 1. The nodes along the top and bottom rows denote the random variables corresponding to the evolving goal and path respectively. The arrows specify interdependencies between the random variables. A consistent prior distribution on the entire set of nodes is provided by specifying distributions for each node conditioned on its parents. Nodes without parents require unconditioned priors. The graphical model imposes a Markov structure, where any node is independent of all other nodes when conditioned on its parents.

While any of a number of graphs might have been drawn to relate path and goal, the specific arrangement of edges depicted in Fig. 1 are consistent with our specifications for a dynamic goal state equation. The graph requires that we define the following densities:

$$p(x_0) \tag{13}$$

$$p(z_0) \tag{14}$$

$$p(x_{t+1} | x_t, z_t) \tag{15}$$

$$p(z_{t+1} | z_t). \tag{16}$$

The priors (13) and (14) are provided by initial uncertainty in the path and goal states. The conditional density represents our intention that the path x_t evolves based on the current goal z_t. This density was identically derived in the static case, and specified by (4). The density (16) allows us to specify the dynamics of the goal exactly as the general linear state equation (12). The goal evolves independently of the path, because the only parent of a goal node is the previous goal node.

With priors (13)–(16) now chosen, the resulting dynamic goal state equation can be expressed as follows:

$$\begin{pmatrix} x_{t+1} \\ z_{t+1} \end{pmatrix} = \begin{pmatrix} \Psi & \Gamma \\ 0 & B_t \end{pmatrix} \begin{pmatrix} x_t \\ z_t \end{pmatrix} + \begin{pmatrix} \varepsilon_t \\ \eta_t \end{pmatrix}. \tag{17}$$

Because the original static goal state equation guarantees that $x_T = z$, the dynamic goal extension (17) ensures that $x_T = z_{T-1}$. To guarantee that x_T and z_T coincide, we must additionally specify that $z_{T-1} = z_T$. This is accomplished by specifying

$$B_{T-1} = I \tag{18}$$

$$\mathrm{var}(\eta_{T-1}) = 0. \tag{19}$$

In practice, we discard the constraints (18) and (19) because of the simplicity in implementing the same set of transition rules (17) for the final sample point.

This dynamic goal state equation (17) closely resembles the static goal state equation (5) because we specifically chose a graphical model that required the conditional density (15) that had previously been derived for static goals in (4). The dynamic goal state equation reduces to the static goal state equation for $B_t = I$ and $\mathrm{var}(\eta_t) = 0$. Both the dynamic and static goal state equations reduce to the free movement state equation (1) as $\mathrm{var}(z_0)$ grows to infinity, and for the dynamic state equation, as var (η_t) grows to infinity.

In summary, the derivation of the dynamic goal state equation begins with the free movement state equation (1). We then explicitly introduced goal dynamics, specifying independent goal evolution with a linear state equation (12). The graphical model (Fig. 1) summarized and unified our constraints. While several alternative choices of directed edges could have been made, this particular graph required the conditional distributions $p(x_{t+1}|x_t, z_t)$ and $p(z_{t+1}|z_t)$ which we had derived in the static goal case and with our goal dynamics (12), respectively. The graphical model specified that that the trajectory variable x_t should evolve to the current notion of goal z_t as if that dynamic goal were the static goal of the moment. Finally, the model described initial arm position and initial goal as independent random variables. On one hand, this appeals to the notion that starting position and goal are unrelated. However, it might be argued that there is a natural dependency between these two variables related to the physical constraints of arm motion. In practice, this point may not be so important because the physically constrained relationship between goal and path are implemented by the first time step as per $p(x_{t+1}|x_t, z_t)$.

In [37], we presented an alternative dynamic goal state equation based on linear quadratic (LQ) control [38]. This is the extension of the control-based static goal case presented in [25], which produced the same average trajectories as the probabilistic static goal equation (5), as discussed more generally by [39]. However, in the dynamic goal control-based extension, the path does not move towards the current notion of goal as in (17), but rather towards the goal as projected into the future through goal dynamics. For the case $B_t = I$, the two state equations have identical average trajectories but different increment variance.

Numerical issues may arise specific to the filter used in combination with the reach state equations. A common situation involves ill-conditioned covariance matrices for the prediction or posterior density of the arm state. In our implementation with the point process filter (see the Appendix), we checked that our covariance matrices were well-conditioned using the Matlab function rcond before inverting. If the prediction density covariance was ill-conditioned, then the posterior density covariance was directly assigned to the prediction density covariance. In the next iteration of the procedure, the covariance of the increment would help make this density well-conditioned. If the posterior density covariance was ill-conditioned on an iteration, then the posterior density covariance formula (24) was altered to remove the $\left(n_k^j - \lambda_k^j \delta_k\right)\left(\partial^2 \log \lambda_k^j / \partial x_k\right)$ term, and recalculated for that iteration. This is equivalent to a Fisher Scoring step.

III. Results

The dynamic goal state equation was evaluated against the static goal and free movement state equations in a series of simulated experiments. Procedures and outcomes are described in Sections III-A–III-D.

A. Sample Trajectories From Dynamic Goal State Equation

Trajectories were generated from the dynamic goal state equation (17) to visualize the assumed structure in intended reaching movements. The state vector x_t included position and velocity terms in a 2-D simulated workspace. Parameters of the reaching movement were assigned as follows, in an attempt to generate realistically proportioned motions. The timestep of the simulation was chosen to be compatible with the point process filtering procedure (see the Appendix) that performs well when a few number of spikes fall in any given time interval. Because firing rates are generally below 50 spikes per second in our simulations, 10-ms timesteps were sufficient. The goal increment covariance corresponds to a goal that moves from its original position with a standard deviation of 7 centimeters over the 2-s reach. Individual covariance values specify the corresponding entries in a diagonal covariance matrix. The initial arm and goal position and velocity covariances are chosen to be small to allow us to observe the effect of accruing uncertainty on the resulting trajectory (see Table I).

Sample trajectories are plotted (Fig. 2). The position trajectories in each axis [Fig. 2(a)] move toward the current goal position, which evolves independently as a random walk. The trajectory velocity profiles [Fig. 2(b)] are approximately bell-shaped, but exhibit high velocity deviations towards the end of the movement in contrast to the static case. The average trajectory of this dynamic goal state equation, indicated in light gray, is indistinguishable from the average trajectory of the static goal case because we have chosen $B_t = I$ in (17). Trajectories that were roughly parabolic under the static goal state equation are now more asymmetric in single trials [Fig. 2(b)]. Velocity profiles exhibit sharp deviations towards the end of the movement in contrast to the static case, because quick corrections must be made to the trajectory based on last-sample changes to the goal. Because we did not implement the final-sample constraints (18) and (19) as a matter of convenience, the goal trajectory z_T is not identical to z_{T-1}, so that when x_T converges to z_{T-1} as per (17), it appears to miss the value z_T. In practice, this incongruence is insignificant, representing error in fractions of a time sample and portions of a millimeter.

TABLE I
MOVEMENT PARAMETERS

Parameter	Baseline Value
Reach distance	0.35 m
Time step	0.01 s
Reach duration	2 s
Goal transition matrix B_t	I
Trajectory position increment variances (part of the cov[ω_t)]	0 m^2 per timestep
Trajectory velocity increment variances (part of the cov[ω_t)]	10^{-4} m^2/s^2 per timestep
Goal position increment variances (part of the cov[η_t)]	2.5×10^{-5} m^2 per timestep
Goal velocity increment variances (part of the cov[η_t)]	0 m^2/s^2 per timestep
Initial arm position (part of z_0)	(0 m, 0 m)
Initial arm velocity (part of z_0)	(0 m/s, 0 m/s)
Initial arm position variances (part of $\mathrm{cov}[\mathrm{z}_0]$	10^{-10} m^2
Initial arm velocity variances (part of $\mathrm{cov}[\mathrm{z}_0]$	10^{-10} m^2/s^2
Initial goal position (part of z_0)	(0.25 m, 0.25 m)
Initial goal velocity (part of z_0)	(0 m/s, 0 m/s)
Initial goal position variances (part of $\mathrm{cov}[\mathrm{z}_0]$	10^{-10} m^2
Initial goal velocity variances (part of $\mathrm{cov}[\mathrm{z}_0]$	10^{-10} m^2/s^2

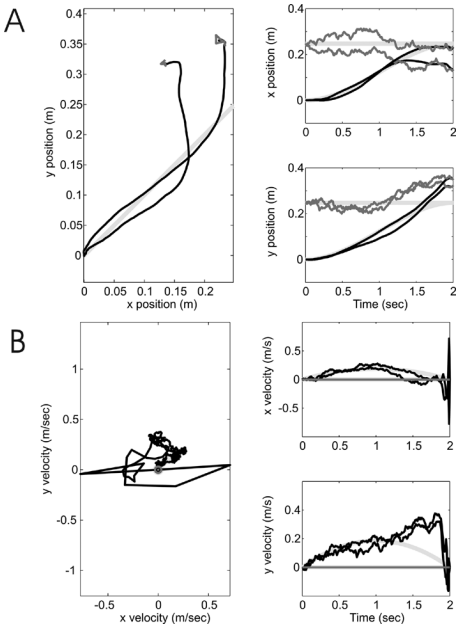

Fig. 2. Sample and average trajectories from the dynamic goal state equation. Goal position (gray) evolves as a random walk, drawing path position (black) towards it. The resulting velocity profiles are still parabolic on average (light gray), indistinguishable from the static case. However, individual path velocity profiles (black) can appear asymmetric with large final excursions that bring the path position to the final goal location.

B. Estimation of Reach Trajectory From Simulated Neural Activity

To evaluate the use of dynamic goal state equations in the prosthetic application, arm trajectories were estimated from a simulated record of neural activity. First, sample arm trajectories were generated according to the control-based dynamic goal state equation (akin to previous section and described in [37]), which produces trajectories very similar to the probabilistic dynamic goal state equation. Trajectories were generated with the parameters tabulated in the previous section, but with goal position increment variance of $10^{-4.8}$ m^2 and initial goal position uncertainty of 10^{-5} m^2.

TABLE II
NEURON TUNING CURVE PARAMETERS

Parameter	Assignment or Interval
β_0	2.28
β_1	4.67 s/m
θ_p	$[-\pi, \pi]$

Next, neural activity from 9 neurons in the form of action potentials, was simulated from these trajectories based on a point process model of primary motor cortical activity [21], [40], [41] using the time-rescaling theorem [42]. The conditional intensity function of these neurons depended on desired velocity

$$\lambda(t|v_x, v_y) = \exp\left(\beta_0 + \beta_1 \left(v_x^2 + v_y^2\right)^{1/2} \cos(\theta - \theta_p)\right) \quad (20)$$

where v_x and v_y are velocities in orthogonal directions. The parameters in (20) determine the turning curve. These parameters were assigned with typical values for primary motor cortex, where the velocity orientation that elicited maximal spiking (θ_p, called the preferred direction) was drawn (independently on each run of the simulation) from a uniform distribution on the interval as shown in Table II.

The corresponding simulated neurons had preferred directions between $-\pi$ and π, background firing rates of 10 spikes/s,

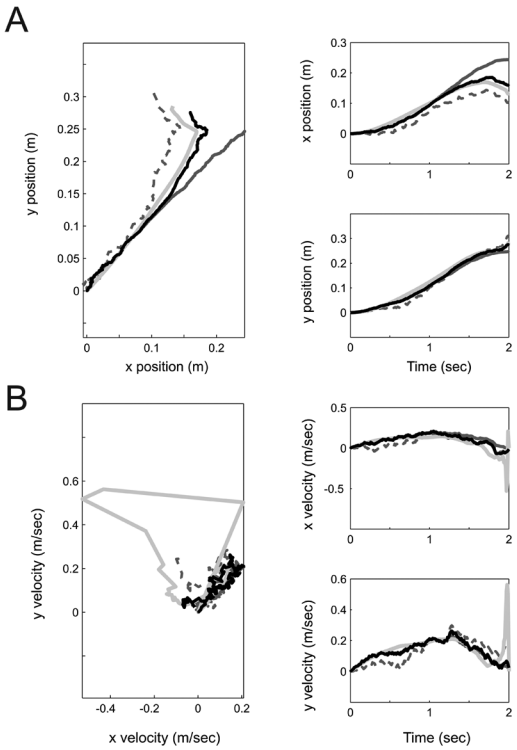

Fig. 3. Estimation of path from ensemble spiking activity of nine simulated motor cortical neurons and a dynamic goal trajectory. Position (A) and velocity (B) estimates from point process filters employing the free movement state equation (dashed), static goal reach state equation (dark gray), and dynamic goal reach state equation (black) are plotted with the true simulated trajectory (light gray). The reach state equations additionally employ one low variance (10^{-10} m^2) observation of the initial goal. The goal position increment variance is $10^{-4.8}$ m^2. See Results for details of simulation procedure.

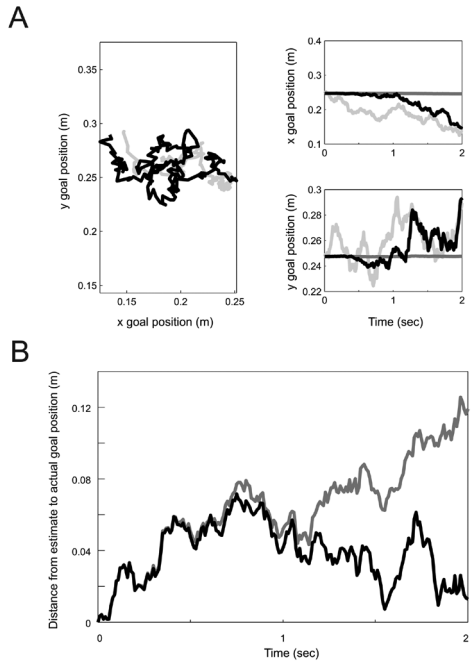

Fig. 4. Estimation of goal from ensemble spiking activity of nine simulated motor cortical neurons and a dynamic goal trajectory. (A) Estimates of the true (light gray) simulated goal trajectory are generated throughout the reach with point process filters using the static goal (dark gray) and dynamic goal (black) state equations. (B) At each time point, the distance between a filter estimate and the actual goal is plotted for the static goal (dark gray) and dynamic goal (black) state equations. The goal position increment variance is $10^{-4.8}$ m^2. See Results for details of simulation procedure.

and firing rates of 24.9 spikes/s at a speed of 0.2 m/s in the θ_p direction.

Finally, a point process filter [21] was used to estimate the reaching movement from the simulated neural activity. This is a recursive estimation procedure that incorporates a state equation and an observation equation that relates neural activity to the trajectory (see the Appendix). The observation equation in our filter was defined by the same conditional intensity function (20) that was used to simulate the neural activity.

Three state equations were evaluated with the point process filter, corresponding to the free movement state equation, static goal state equation, and dynamic goal state equation (Fig. 3). The decoding goal increment variance was $10^{-4.8}$ m^2 per timestep, equal to the trajectory-generating variance for that trial.

The resulting difference between static and dynamic goal state equations is especially apparent when the initial uncertainty in goal location is small (Fig. 3). In that case, the static goal state equation largely disregards motor cortical activity in updating estimates of goal location. Consequently, the reconstructed static goal state equation trajectory persists towards the goal location indicated by the initial observation of goal. Large mean square errors (MSEs) are accumulated as the static goal state equation fails to incorporate motor cortical observations that would otherwise reorient its goal estimates. Attempts to compensate this effect by increasing the initial goal uncertainty in the static goal state equation result in large, rapid excursions in the initial goal estimates [28]. In contrast, the dynamic goal state equation, with the same small initial uncertainty in goal location, gradually down weights the initial goal observation over the reach, and progressively incorporates motor cortical observations. With the appropriate choice of goal increment variance, the dynamic goal state equation uses the initial goal observation to outperform the free movement state equation early in the reach, and incorporates motor cortical activity to outperform the static goal state equation later in the reach.

C. Estimation of Reach Goal From Simulated Neural Activity

As with the static goal state equation, filters based on the dynamic goal state equation provide estimates of the goal throughout the reaching movement. We compare goal reconstruction between static and dynamic goal state equations over the entire duration of one reach (Fig. 4). The dynamic goal state equation estimates of the goal track the actual goal movement in the 2-D workspace [Fig. 4(a)]. The Euclidean distances between the static goal or dynamic goal estimates and the actual goal location are plotted for each time point [Fig. 4(b)].

Early in the movement, static goal and dynamic goal errors are indistinguishable for two reasons. First, the goal is distant in time, so that the trajectory increments are not strongly affected by the goal location. Second, the dynamic goal state equation has not yet sufficiently down weighted the initial goal observation. As with the static goal state equation, dynamic goal state equation estimates must balance path-related activity against the initial goal-related activity in producing estimates of goal and path. One-second after the start of the trajectory, the static goal increments are more driven by the original goal location, whereas the dynamic goal state equation has down weighted

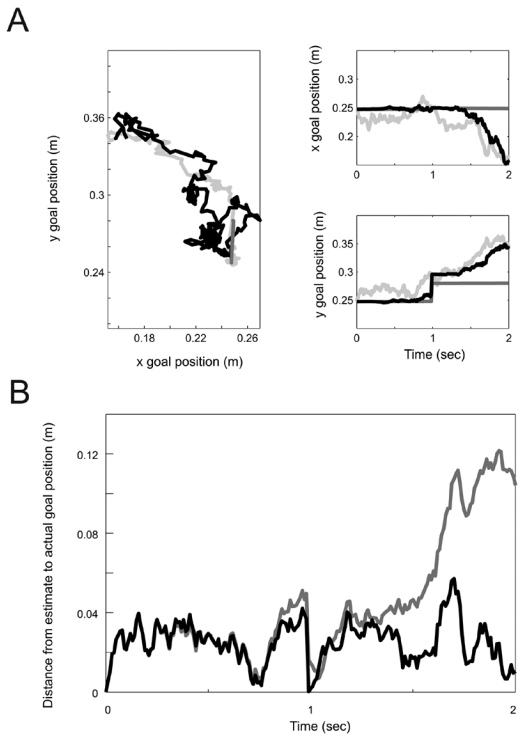

Fig. 5. Incorporating mid-reach goal observations from a simulated online goal correction region in parietal cortex. Estimates of goal are generated as with Fig. 4, but 1 s into the reach, low variance (10^{-5} m^2 position, 10^{-7} m^2 velocity) observations of the goal are available to both static goal (dark gray) and dynamic goal (black) point process filters. Again, position estimates are plotted with the actual (light gray) goal trajectory (A), and distances between estimated and actual goal trajectories are calculated over the duration of the reach (B). The goal position increment variance is $10^{-4.8}$ m^2. See Results for details of simulation procedure.

that initial observation and incorporated path-related activity to guide its estimates. As a result, the dynamic goal estimate errors remain closer to the true goal location than static goal estimate errors. Goal decoding results are compared along each of the two cardinal directions in the workspace [Fig. 4(a), right panels]. The static goal state equation fails to follow the moving goal, while the dynamic goal state equation is able to incorporate path-related activity to update its goal estimates.

D. Incorporation of Information From Dynamic Goal Planning Regions

The possibility of incorporating additional observations of goal during the reach from parietal cortical areas [29], [33] was investigated (Fig. 5). A Gaussian observation of the goal location was introduced 1 s into the reach, using a diagonal observation covariance matrix with position observation noise variance 10^{-5} m^2, and velocity observation noise variance 10^{-7} m^2.

Goal estimates were then generated as in the previous section, but now informed by this additional observation of goal location (Fig. 5). A sharp correction of the goal estimate is made at the 1-s mark where the additional observation is incorporated [Fig. 5(a)]. The distance between estimated and actual goal position collapses towards zero at 1 s, reflecting the estimate correction [Fig. 5(b)].

The dynamic goal state equation may be better able to incorporate additional observations of a changing goal than the static goal state equation. This is because the dynamic state equation gradually increases goal estimate uncertainty in anticipation of a moving goal, allowing new observations of the goal to correct old estimates to a larger extent than the static goal state equation. Recent empirical results [29], [33] suggest brain-driven interfaces that record from parietal areas [7] may have ready access to these additional observations of a dynamic goal during the course of a reach.

E. Characterizing MSE

The average reconstruction performance of the free movement, static goal, and dynamic goal state equations was then compared over a range of goal position increment variances using a simulated population of 9 primary motor neurons, an easily achievable population size with chronic recording technologies. MSE was calculated for estimates of trajectory position, desired goal position over the entire reach, and desired goal position at the endpoint of the reach.

For each goal increment variance, MSEs were averaged over 100 independently simulated trajectories, with new tuning curve parameters chosen on every trial for each of the 9 neurons. The goal position increment variance of the dynamic goal state equation used in the filter was chosen to be equal to that of the trajectory-generating state equation.

The dynamic goal state equation performs no worse on average than the free movement and static goal state equations for all three measures of MSE (Fig. 6). This is because the dynamic goal state equation can be set to correspond to the static goal and free movement state equations by choosing zero goal increment variance and large goal increment variance respectively. In an intermediate regime of goal movement, the dynamic goal state equation outperforms both alternative methods.

Why consider MSE of goal estimates at all? The premise of a goal-directed movement is that the performance index that matters most to the user is the accuracy, speed, and effort with which the goal is acquired. Consequently, the MSE of the goal reconstruction is possibly more relevant to the user than the MSE of the path reconstruction. This is in contrast to evaluating brain-driven interfaces for free movement, where the primary figure of merit is related to the MSE of path reconstruction.

IV. Discussion

We have developed a method for driving reaching arm movements to a dynamic goal using neural activity. The dynamic goal state equation is the central component of this method that involves recursive estimation of an intended movement from ongoing observations of neural activity that relate to path and goal. The approach represents a generalization of brain-driven interfaces that support free arm movement [1]–[5], [17] and movement to a static goal [24]–[28].

If the relevant performance criterion is goal acquisition, then why should reach state equations include state variables that correspond to the path? In the context of the static goal state equation, this allows the incorporation of path-related neural activity (such as from primary motor cortex), in order to refine estimates of the goal location. In the dynamic goal state equation, state variables that represent the path enable a far more dramatic ability. The goal can now be steered over the entire duration of the reach with path related activity and online goal-correction areas. The goal increment variance can be tuned to achieve an

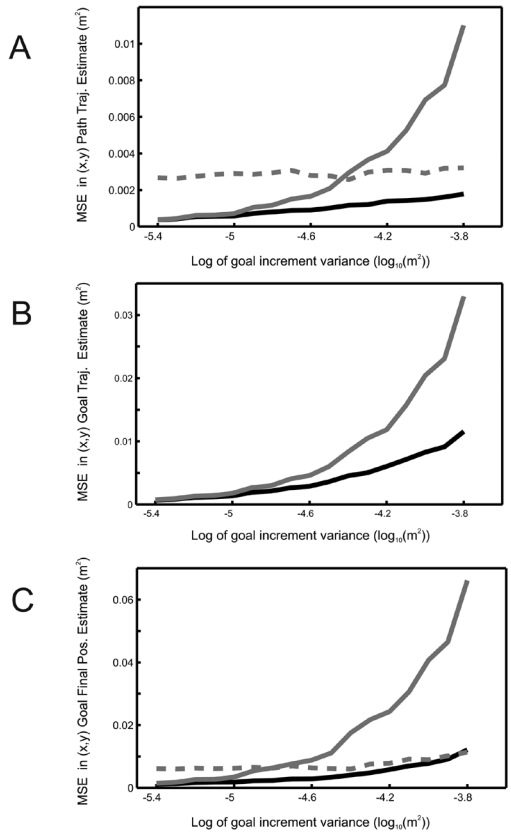

Fig. 6. MSE in estimates of (A) path position, (B) goal position trajectory, and (C) goal final position, as a function of goal increment variance, with a simulated population of 9 motor cortical neurons. MSE was calculated over 100 trials for each simulation goal increment variance using point process filters with the free movement state equation (dashed), static goal state equation (dark gray), and dynamic goal state equation (black). Goal position trajectory estimates (B) are not supported by the free movement state equation.

optimal tradeoff point between smooth control and responsive tracking of goal state.

Although estimates of the path were demonstrated and evaluated in this paper as well as in earlier work on the static case, it is not necessary that these estimates be used in controlling a goal-directed movement. Instead, an independent control algorithm could plan the trajectory of the device from its initial state to the goal state. The role of the user would then entirely be concentrated in specifying the goal state. Control theory and on-board sensor data could be integrated for trajectory routing. This approach would allow high-performance trajectory navigation in complex environments (such as with obstacles) even with small neural ensembles or broadly tuned local field potentials that limit the precise and direct specification of a trajectory. Because the goal state is necessarily linked to the path, the user would still feel capable of steering the trajectory via control over a dynamic goal state.

V. Conclusion

Brain-driven interfaces allow a user to generate neural activity to specify command signals for assistive devices like typing software or robotic arms. These neural prostheses are expected to enable individuals with severe motor deficits to recover function. Previously, a state equation was derived to enable users to specify both goal and path in the control of reaching movements to a static goal. This paper extended the static goal state equation to dynamic goals that change over the course of a reach, demonstrated the incorporation of online goal-related activity, introduced the use of goal-reconstruction MSE, and proposed a framework to integrate sensors and control theory into the coordination of an assistive device.

The dynamic goal approach utilizes information about a changing goal [29], [33] that may already be accessible to brain-driven interface prototypes that monitor parietal cortex [7]. By incorporating these brain signals, the dynamic goal state equation affords new functionality to the user without additional hardware development or surgical intervention. Even when these additional signals are not available, the method better tracks reaching to moving goals, and allows an intermediate level of control between movements to a static goal and free arm movements.

The control of reaching to dynamic goals in brain-driven interfaces will benefit from three specific advances. First, the electrophysiological characterization of online goal-correction areas would allow for direct observations of the changing goal, where primary motor path-related activity currently serves as an indirect surrogate. Second, switching filters, non-Gaussian density propagation, or other methods related to detection of change would allow better tracking of goals that move suddenly between intervals of relative stasis. This is a particularly difficult task in the present realization, because nonzero goal increment variances that are needed to track changes also cause drifting in periods where the goal is static. Third, more reliable dynamic goal estimates are expected from planning or trajectory-related regions with a discrete goal set. We hope to explore these avenues of development in subsequent work.

Appendix
Filtering Spikes or Field Potentials With State Equations

The static and dynamic goal state equations discussed in this paper are compatible with any recursive Bayesian estimation procedure like the Kalman filter [22], particle filter [20], and point process filter [21]. For convenience, we provide a summary of the prediction and update equations of the point process filter that was used in our illustration of estimation with neuronal spiking activity and the static and dynamic goal state equations. A detailed exposition on this point process filter can be found in [21]. Also as described below, this procedure can be modified to accommodate Gaussian (instead of point process) observations for field potentials like EEG and LFP.

Consider a state equation that corresponds to the following state transition density:

$$p(x_{k+1}|x_k) \sim N(F_k x_k + b_k, Q_k) \tag{21}$$

and the point process observation model based on (20) that specifies the instantaneous probability of spiking from the jth primary motor neuron, in terms of the conditional intensity function, λ_k^j, to denote dependence on the current arm state x_k. Define δ_k to be the length of the kth discrete time interval, and n_k^j to be the number of spikes generated by the jth neuron in that time interval.

The prediction density mean $x_{k+1|k}$ and covariance $\Lambda_{k+1|k}$ are given by

$$x_{k+1|k} = F_k x_{k|k} + b_k \tag{22}$$

$$\Lambda_{k+1|k} = F_k \Lambda_{k|k} F_k' + Q_k \tag{23}$$

The posterior density covariance $\Lambda_{k+1|k+1}$ and mean $x_{k+1|k+1}$ are

$$\begin{aligned}(\Lambda_{k+1|k+1})^{-1} &= (\Lambda_{k+1|k})^{-1} \\ &\quad + \sum_{j=1}^{C}\left[\left(\frac{\partial \log \lambda_k^j}{\partial x_k}\right)'\left[\lambda_k^j \delta_k\right]\right. \\ &\qquad \left(\frac{\partial \log \lambda_k^j}{\partial x_k}\right) - \left(n_k^j - \lambda_k^j \delta_k\right) \\ &\qquad \left.\times \frac{\partial^2 \log \lambda_k^j}{\partial x_k \partial x_k'}\right]_{x_{k+1|k}}\end{aligned} \tag{24}$$

$$\begin{aligned}x_{k+1|k+1} &= x_{k+1|k} + \Lambda_{k+1|k+1} \\ &\quad \times \sum_{j=1}^{C}\left[\left(\frac{\partial \log \lambda_k^j}{\partial x_k}\right)'\left(n_k^j - \lambda_k^j \delta_k\right)\right]_{x_{k+1|k}}\end{aligned} \tag{25}$$

The Kalman filter is the corresponding approach if instead, the array of C neural signals $\underline{n}_k = \left[n_{k+1}^1, n_{k+1}^2, \ldots, n_{k+1}^C\right]'$ is described by a Gaussian observation model (such as EEG) with mean $D_k x_k + f_k(H_k)$ and variance W_k. Here, x_k is a $J \times 1$ vector of continuous states, D_k is a $C \times J$ matrix, and $f_k(H_k)$ is a function that maps neural history to a $C \times 1$ vector, such as with ARMA models. The posterior density covariance and mean are then given by the standard Kalman filter equations [50]

$$\begin{aligned}\Lambda_{k+1|k+1} &= \Lambda_{k+1|k} - \Lambda_{k+1|k} D_{k+1}' \\ &\quad \times \left(D_{k+1} \Lambda_{k+1|k} D_{k+1}' + R_{k+1}\right)^{-1} D_{k+1} \Lambda_{k+1|k}\end{aligned} \tag{26}$$

$$\begin{aligned}x_{k+1|k+1} &= x_{k+1|k} + \Lambda_{k+1|k} D_{k+1}' \\ &\quad \times \left(D_{k+1} \Lambda_{k+1|k} D_{k+1}' + R_{k+1}\right)^{-1} \\ &\quad \times \left(\underline{n}_{k+1} - D_{k+1} x_{k+1|k} - f_{k+1}(H_{k+1})\right).\end{aligned} \tag{27}$$

ACKNOWLEDGMENT

L. Srinivasan would like to thank J. Johnson, D. Malioutov, and U. T. Eden for discussions.

REFERENCES

[1] J. R. Wolpaw and D. J. McFarland, "Control of a two-dimensional movement signal by a noninvasive brain-computer interface in humans," *Proc. Nat. Acad. Sci. USA*, vol. 101, pp. 17849–17854, 2004.

[2] E. C. Leuthardt, G. Schalk, J. R. Wolpaw, J. G. Ojemann, and D. W. Moran, "A brain-computer interface using electrocorticographic signals in humans," *J. Neural Eng.*, vol. 1, pp. 63–71, 2004.

[3] J. M. Carmena, M. A. Lebedev, R. E. Crist, J. E. O'Doherty, D. M. Santucci, D. F. Dimitrov, P. G. Patil, C. S. Henriquez, and M. A. Nicolelis, "Learning to control a brain-machine interface for reaching and grasping by primates," *PLoS Biol.*, vol. 1, pp. E42–E42, 2003.

[4] M. D. Serruya, N. G. Hatsopoulos, L. Paninski, M. R. Fellows, and J. P. Donoghue, "Instant neural control of a movement signal," *Nature*, vol. 416, pp. 141–142, 2002.

[5] D. M. Taylor, S. I. Tillery, and A. B. Schwartz, "Direct cortical control of 3D neuroprosthetic devices," *Science*, vol. 296, pp. 1829–1832, 2002.

[6] K. V. Shenoy, D. Meeker, S. Cao, S. A. Kureshi, B. Pesaran, C. A. Buneo, A. P. Batista, P. P. Mitra, J. W. Burdick, and R. A. Andersen, "Neural prosthetic control signals from plan activity," *Neuroreport*, vol. 14, pp. 591–596, 2003.

[7] S. Musallam, B. D. Corneil, B. Greger, H. Scherberger, and R. A. Andersen, "Cognitive control signals for neural prosthetics," *Science*, vol. 305, pp. 258–262, 2004.

[8] T. A. Kuiken, G. A. Dumanian, R. D. Lipschutz, L. A. Miller, and K. A. Stubblefield, "Targeted muscle reinnervation for improved myoelectric prosthesis control," in *Proc. 2nd Int. IEEE EMBS Conf. Neural Engineering*, 2005, pp. 396–399.

[9] D. D. Frey, L. E. Carlson, and V. Ramaswamy, "Voluntary-Opening prehensors with adjustable grip force," *J. Prosth. Orthotics*, vol. 7, pp. 124–131, 1995.

[10] W. J. Freeman, M. D. Holmes, B. C. Burke, and S. Vanhatalo, "Spatial spectra of scalp EEG and EMG from awake humans," *Clin. Neurophysiol.*, vol. 114, pp. 1053–1068, 2003.

[11] E. H. D'Hollander and G. A. Orban, "Spike recognition and on-line classification by unsupervised learning system," *IEEE Trans. Biomed. Eng.*, vol. BME-26, pp. 279–284, 1979.

[12] F. Worgotter, W. J. Daunicht, and R. Eckmiller, "An on-line spike form discriminator for extracellular recordings based on an analog correlation technique," *J. Neurosci. Meth.*, vol. 17, pp. 141–151, 1986.

[13] M. S. Fee, P. P. Mitra, and D. Kleinfeld, "Automatic sorting of multiple unit neuronal signals in the presence of anisotropic and non-Gaussian variability," *J. Neurosci. Meth.*, vol. 69, pp. 175–188, 1996.

[14] R. Chandra and L. M. Optican, "Detection, classification, and superposition resolution of action potentials in multiunit single-channel recordings by an on-line real-time neural network," *IEEE Trans. Biomed. Eng.*, vol. 44, no. 5, pp. 403–412, May 1997.

[15] U. T. Eden, W. Truccolo, M. R. Fellows, J. P. Donoghue, and E. N. Brown, "Reconstruction of hand movement trajectories from a dynamic ensemble of spiking motor cortical neurons," in *Proc. 26th IEEE Engineering in Medicine and Biology Society Annu. Conf. (EMBC '04)*, 2004, vol. 2, pp. 4017–4020.

[16] L. R. Hochberg, M. D. Serruya, G. M. Friehs, J. A. Mukand, M. Saleh, A. H. Caplan, A. Branner, D. Chen, R. D. Penn, and J. P. Donoghue, "Neuronal ensemble control of prosthetic devices by a human with tetraplegia," *Nature*, vol. 442, pp. 164–171, 2006.

[17] J. R. Wolpaw and D. J. McFarland, "Multichannel EEG-based brain-computer communication," *Electroencephalogr. Clin. Neurophysiol.*, vol. 90, pp. 444–449, 1994.

[18] A. P. Georgopoulos, A. B. Schwartz, and R. E. Kettner, "Neuronal population coding of movement direction," *Science*, vol. 233, pp. 1416–1419, 1986.

[19] J. Wessberg, C. R. Stambaugh, J. D. Kralik, P. D. Beck, M. Laubach, J. K. Chapin, J. Kim, S. J. Biggs, M. A. Srinivasan, and M. A. Nicolelis, "Real-time prediction of hand trajectory by ensembles of cortical neurons in primates," *Nature*, vol. 408, pp. 361–365, 2000.

[20] A. E. Brockwell, A. L. Rojas, and R. E. Kass, "Recursive bayesian decoding of motor cortical signals by particle filtering," *J. Neurophysiol.*, vol. 91, pp. 1899–1907, 2004.

[21] U. T. Eden, L. M. Frank, R. Barbieri, V. Solo, and E. N. Brown, "Dynamic analysis of neural encoding by point process adaptive filtering," *Neural Comput.*, vol. 16, pp. 971–998, 2004.

[22] W. Wu, Y. Gao, E. Bienenstock, J. P. Donoghue, and M. J. Black, "Bayesian population decoding of motor cortical activity using a Kalman filter," *Neural Comput.*, vol. 18, pp. 80–118, 2006.

[23] R Barbieri, M. A. Wilson, L. M. Frank, and E. N. Brown, "An analysis of hippocampal spatio-temporal representations using a Bayesian algorithm for neural spike train decoding," *IEEE Trans. Neural Syst. Rehabil. Eng.*, vol. 13, no. 2, pp. 131–136, 2005.

[24] T. M. Cowan and D. M. Taylor, "Predicting reach goal in a continuous workspace for command of a brain-controlled upper-limb neuroprosthesis," in *Proc. 2nd Int. IEEE EMBS Conf. Neural Engineering*, 2005, pp. 74–74.

[25] C. Kemere and T. H. Meng, "Optimal estimation of feed-forward-controlled linear systems," in *Proc IEEE Int. Conf. Acoustics, Speech and Signal Processing (ICASSP '05)*, 2005, vol. 5, pp. 353–356.

[26] L. Srinivasan, U. T. Eden, A. S. Willsky, and E. N. Brown, "Goal-directed state equation for tracking reaching movements using neural signals," in *Proc. 2nd Int. IEEE EMBS Conf. Neural Engineering*, 2005, pp. 352–355.

[27] B. M. Yu, G. Santhanam, S. I. Ryu, and K. V. Shenoy, "Feedback-directed state transition for recursive bayesian estimation of goal-directed trajectories," in *Computational and Systems Neuroscience (COSYNE) Meeting Abstract*, Salt Lake City, UT, 2005.
[28] L. Srinivasan, U. T. Eden, A. S. Willsky, and E. N. Brown, "A state-space analysis for reconstruction of goal-directed movements using neural signals," *Neural Computation*, vol. 10, no. 18, 2006.
[29] H. Merchant, A. Battaglia-Mayer, and A. P. Georgopoulos, "Neural responses during interception of real and apparent circularly moving stimuli in motor cortex and area 7a," *Cereb. Cortex*, vol. 14, pp. 314–331, 2004.
[30] J. F. Soechting and F. Lacquaniti, "Modification of trajectory of a pointing movement in response to a change in target location," *J. Neurophysiol.*, vol. 49, pp. 548–564, 1983.
[31] T. E. Milner and M. M. Ijaz, "The effect of accuracy constraints on three-dimensional movement kinematics," *Neuroscience*, vol. 35, pp. 365–374, 1990.
[32] D. Lee, N. L. Port, and A. P. Georgopoulos, "Manual interception of moving targets. II. On-line control of overlapping submovements," *Exp. Brain Res.*, vol. 116, pp. 421–433, 1997.
[33] M. Desmurget, C. M. Epstein, R. S. Turner, C. Prablanc, G. E. Alexander, and S. T. Grafton, "Role of the posterior parietal cortex in updating reaching movements to a visual target," *Nat. Neurosci.*, vol. 2, pp. 563–567, 1999.
[34] A. P. Batista, C. A. Buneo, L. H. Snyder, and R. A. Andersen, "Reach plans in eye-centered coordinates," *Science*, vol. 285, pp. 257–260, 1999.
[35] W. P. Medendorp, H. C. Goltz, T. Vilis, and J. D. Crawford, "Gaze-centered updating of visual space in human parietal cortex," *J. Neurosci.*, vol. 23, pp. 6209–6214, 2003.
[36] A. Z. Khan, L. Pisella, A. Vighetto, F. Cotton, J. Luaute, D. Boisson, R. Salemme, J. D. Crawford, and Y. Rossetti, "Optic ataxia errors depend on remapped, not viewed, target location," *Nat. Neurosci.*, vol. 8, pp. 418–420, 2005.
[37] L. Srinivasan and E. N. Brown, "Dynamic-goal state equations for tracking reaching movements using neural signals," in *Proc. 1st IEEE RAS-EMBS Int. Conf. Biomed Robotics and Biomechatronics (BioRob '06)*, 2006.
[38] D. P. Bertsekas, *Dynamic Programming and Optimal Control*, 3rd ed. MA, Belmont: Athena Scientific, 2005.
[39] T. Kailath, A. H. Sayed, and B. Hassibi, *Linear Estimation*. Upper Saddle River, NJ: Prentice-Hall, 2000.
[40] D. W. Moran and A. B. Schwartz, "Motor cortical representation of speed and direction during reaching," *J. Neurophysiol.*, vol. 82, pp. 2676–2692, 1999.
[41] W. Truccolo, U. T. Eden, M. R. Fellows, J. P. Donoghue, and E. N. Brown, "A point process framework for relating neural spiking activity to spiking history, neural ensemble, and extrinsic covariate effects," *J. Neurophysiol.*, vol. 93, pp. 1074–1089, 2005.
[42] E. N. Brown, R. Barbieri, V. Ventura, R. E. Kass, and L. M. Frank, "The time-rescaling theorem and its application to neural spike train data analysis," *Neural Comput.*, vol. 14, pp. 325–346, 2002.

Lakshminarayan Srinivasan (M'05) received the B.S. degree in electrical and computer engineering (with honors) from the California Institute of Technology, Pasadena, CA, and the S.M. and Ph.D. degrees, both in electrical engineering and computer science from the Massachusetts Institute of Technology, Cambridge. He is currently a candidate for the M.D. degree at the Harvard Medical School, Health Sciences & Technology track.

He is currently a postdoctoral Research Fellow in neurosurgery at the Center for Nervous System Repair, Massachusetts General Hospital. He is broadly interested in the analysis and design of neural systems. The current focus of his research is the probabilistic description of the sensorimotor nervous system, and the development of brain-machine interfaces for communication and control.

Dr. Srinivasan was awarded the National Science Foundation Graduate Research Fellowship (2002) and MIT Presidential Fellowship (2002). Previously, he was the recipient of the Henry Ford II Scholar Award for academic excellence at Caltech (2001), and the Donald S. Clark Award for service to the Caltech community (2001). He was also awarded the Neuroscience Prize, presented by the American Academy of Neurology & Child Neurology Society (1998). His other distinctions include the Bank of America Joe Martin Award of Excellence (1998) and the Captain John Skinner Award from the Armed Forces Communications and Electronics Association (1998).

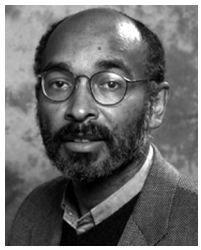

Emery N. Brown (M'01–SM'06) received the B.A. degree from Harvard College, Cambridge, MA, the M.D. degree from Harvard Medical School, Boston, MA, and the A.M. and Ph.D. degrees in statistics from Harvard University, Cambridge, MA.

He is presently Professor of Computational Neuroscience and Health Sciences and Technology in the Department of Brain and Cognitive Sciences and the MIT-Division of Health Sciences and Technology at Massachusetts Institute of Technology, Professor of Anaesthesia at Harvard Medical School, and Director of the Neuroscience Statistics Research Laboratory and an Anesthesiologist in the Department of Anesthesia and Critical Care at Massachusetts General Hospital. His research interests are in the development of signal processing algorithms and point process methods for the analysis of neural systems.

Dr. Brown is a member of the Association of University of Anesthesiologists and of the Committee of Applied and Theoretical Statistics of the National Academies. He is a fellow of the American Institute of Medical and Biological Engineering, and of the American Statistical Association.